Prominin-1 Localizes to the Open Rims of Outer Segment Lamellae in *Xenopus laevis* Rod and Cone Photoreceptors

Zhou Han,[1,2] *David W. Anderson,*[1] *and David S. Papermaster*[1]

Purpose. Prominin-1 expresses in rod and cone photoreceptors. Mutations in the prominin-1 gene cause retinal degeneration in humans. In this study, the authors investigated the expression and subcellular localization of xlProminin-1 protein, the *Xenopus laevis* ortholog of prominin-1, in rod and cone photoreceptors of this frog.

Methods. Antibodies specific for xlProminin-1 were generated. Immunoblotting was used to study the expression and posttranslational processing of xlProminin-1 protein. Immunocytochemical light and electron microscopy and transgenesis were used to study the subcellular distribution of xlProminin-1.

Results. xlProminin-1 is expressed and is subject to posttranslational proteolytic processing in the retina, brain, and kidney. xlProminin-1 is differently expressed and localized in outer segments of rod and cone photoreceptors of *X. laevis*. Antibodies specific for the N or C termini of xlProminin-1 labeled the open rims of lamellae of cone outer segments (COS) and the open lamellae at the base of rod outer segments (ROS). By contrast, anti–peripherin-2/rds antibody, Xper5A11, labeled the closed rims of cone lamellae adjacent to the ciliary axoneme and the rims of the closed ROS disks. The extent of labeling of the basal ROS by anti–xlProminin-1 antibodies varied with the light cycle in this frog. The entire ROS was also faintly labeled by both antibodies, a result that contrasts with the current notion that prominin-1 localizes only to the basal ROS.

Conclusions. These findings suggest that xlProminin-1 may serve as an anti–fusogenic factor in the regulation of disk morphogenesis and may help to maintain the open lamellar structure of basal ROS and COS disks in *X. laevis* photoreceptors. (*Invest Ophthalmol Vis Sci.* 2012;53:361–373) DOI:10.1167/iovs.11-8635

The extraordinary compartmentalization of rod and cone photoreceptors has long drawn attention. Their unique light-sensitive organelles, termed outer segments (OS), respond to varied wavelengths of the visual spectrum.[1] Outer segments are both biochemically and biosynthetically distinct organelles that connect to the cell body (the inner segment [IS]) by a narrow 9+0 nonmotile connecting cilium.[2–4] For more than 100 years, the pathways of photoexcitation and the anatomic structures in rods and have been found to be parallel but distinct.[5] Rods are more sensitive to dim light, typically in the blue-green region of the visual spectrum, whereas cones respond to long (red-orange), intermediate (blue-green), and short (blue-purple) regions of the visual spectrum[6,7] as a consequence of their expression of various opsin genes.[8] In addition, rods and cones have distinct morphologies. Rod photoreceptors have long cylindrical OS consisting of a stack of disks surrounded by, but separate from, the plasma membrane that encases them. Only at the base do the disks assume a lamellar shape with continuity between the lamellar surface and the plasma membrane.[9] By contrast, in frogs and lower vertebrates in general, the cone outer segment (COS) are conical and the lamellae do not separate from the plasma membrane, so that the interlamellar space is permeable to extracellular molecules.[10] In higher vertebrates, the COS lamellae are largely isolated within the enclosing plasma membrane and undergo episodic fusion with it to become accessible to extracellular molecular penetration for reasons that are undefined.[11–14]

This anatomic difference has consequences for the renewal of rod and cone OS membranes. Newly synthesized rhodopsin is deposited into the basal lamellae of growing rod outer segment (ROS) but then becomes locked into the disk as it separates from the plasma membrane and is moved outward by formation of new disks below.[15,16] Newly inserted cone opsins, by contrast, distribute throughout the length and breadth of the COS as a consequence of the continuity of the lamellae and plasma membrane.[10,17] ROS disk protein remains confined within a given disk until it arrives at the top of the stack and is then shed and engulfed into the adjacent pigment epithelial cells.[18–20] Thus the morphogenesis of these highly related organelles poses distinct challenges to interpret how rods and cones accomplish the sculpting and renewal of two such distinct structures. Moreover, the entire process of morphogenesis occurs at the distal tip of the connecting cilium that connects the OS to the inner segment (IS), so that much of the cells' machinery is unavailable to accomplish this task. It has long been suspected that unidentified proteins account for this difference.

Prominin-1, a pentaspan transmembrane protein,[21–23] may be a candidate that participates in the morphogenesis or maintenance of OS structure in rod and cone photoreceptors. Maw et al.[24] discovered that prominin-1 is localized to the evaginations of the plasma membrane that form the new basal lamellae at the base of murine ROS. Zacchigna et al.[25] reported that knocking out prominin-1 in mice causes progressive degeneration of the photoreceptors, as evidenced by thinning of the outer nuclear layer. It is not clear whether cones also degenerate, but cone opsin missorting is observed in prominin$^{-/-}$ mice, and the morphology of both ROS and COS is abnormal

From the [1]Department of Neuroscience, University of Connecticut Health Center, Farmington, Connecticut.

[2]Present affiliation: The John B. Pierce Laboratory, Yale University, New Haven, Connecticut.

Supported by National Institutes of Health Grant EY6891 (DSP) and the John A. and Florence Mattern Solomon Chair in Vision Research and Eye Diseases (DSP).

Submitted for publication September 20, 2011; revised October 20, 2011; accepted October 25, 2011.

Disclosure: **Z. Han**, None; **D.W. Anderson**, None; **D.S. Papermaster**, None

Corresponding author: David S. Papermaster, Department of Neuroscience, University of Connecticut Health Center, 263 Farmington Avenue, Farmington, CT 06032-3401; dspprmstr@gmail.com.

before the cells die. A frameshift mutation ($PROML1_{1878}$, now designated c.1841delG) of prominin-1 is responsible for an autosomal recessive retinal degeneration in a consanguineous Indian family.[24] An autosomal dominant mutation, R373C, of prominin-1 in humans caused retinal degeneration and abnormal structure of ROS in mice carrying this mutation.[26] A third mutation, c.869delG, of human prominin-1 causes autosomal recessive retinitis pigmentosa in patients.[27] However, despite these studies, little is known about the precise localization and the function of prominin-1 in photoreceptors.

In *Drosophila melanogaster*, prominin was found to bind to spacemaker (spam), an intercellular glycoprotein.[28] In the presence of spacemaker, the fly's rhabdomeres are separated. However, in insects not expressing spacemaker (for example, *Apis mellifera*, the honeybee), rhabdomeres adhere to each other, thereby participating in the two alternative arrangements of the compound eye's photoreceptors.[28] Mammalian agrin and perlecan share similarity with the C terminus of spacemaker,[28] but no homolog of spacemaker has yet been identified in vertebrates. These intriguing findings suggest that prominin may bind to extracellular proteins in the vicinity of the ROS basal disks or COS lamellae in vertebrates as well. Besides the expected interacting partners of prominin-1 in the extracellular space, photoreceptor cadherin 21 (PCDH21), a transmembrane protein, and filamentous actin, an intracellular protein, were found to bind to prominin-1 in mice.[26]

Why prominin-1 distributes to the ROS basal lamellae and how it is retained there is unknown, since it is reported to be excluded from the mature upper disks. Distribution of prominin-1 in the continuous membrane system of the COS has not been previously examined by high-resolution techniques. Prominin-1 has recently been observed at the base of COS in mice,[25] but without much detail of its subcellular localization, probably because of the small diameters of murine COS.

We recently described the cloning of three homologs of prominin in *Xenopus laevis*: xlProminin-1, xlProminin-2, and xlProminin-3.[29] xlProminin-1 was identified as the ortholog of prominin-1 in this frog by phylogenetic analysis and was found to be expressed in the retina.[29] In the present study, we generated antibodies against xlProminin-1 and studied its protein expression in *X. laevis* tissues with immunoblotting. We also used fluorescence and electron microscopic immunocytochemical methods to localize prominin-1 in *X. laevis* photoreceptors. We present evidence that xlProminin-1 localizes to the open rims of COS lamellae and open basal lamellae of ROS. We then generated transgenic *X. laevis* expressing the xlProminin-1-hrGFP II fusion protein in either rods or cones by using cell-specific promoters. Comparison of results obtained in transgenic *X. laevis* tadpoles and immunolocalization in normal tadpoles allowed us to evaluate the distribution of the transgene product independently.

Materials and Methods

Animals

Adult *X. laevis* were purchased from *Xenopus* Express (Brooksville, FL). *X. laevis* tadpoles were generated by restriction enzyme-mediated integration transgenesis.[36,38] Animals were kept in an artificially controlled 12-hour light/12-hour dark environment at a constant temperature of 18°C. The light intensity of the light phase was kept at 500 ± 100 lux. All experiments were conducted in accordance with the Animal Care and Use Committee of the University of Connecticut Health Center and the ARVO Statement for the Use of Animals in Ophthalmic and Vision Research.

Polyclonal Antibody Generation

Rabbits were immunized with polypeptides from N and C termini of xlProminin-1 (PN and PC) fused to the C terminus of glutathione S-transferase (GST) as immunogens (Table 1). cDNA fragments coding for PN and PC were amplified by PCR and were inserted into the pGEX-5X2 vector (Amersham, Little Chalfont, UK). Fusion proteins expressed in *Escherichia coli* strain BL21 (DE3) were isolated by binding to glutathione-coupled Sepharose 4B beads (Amersham) and elution with glutathione. Purified fusion proteins were mixed with adjuvant (Ribi Adjuvant System; Corixa Corporation, Seattle, WA) to a final concentration of 0.2 mg/mL and were used to immunize New Zealand White female rabbits (each weighing ~3 kg) with a series of injections over several months.

Expression and Purification of Fusion Protein from Bacterial Cell Lysis

Six constructs (MBP-PN, MBP-612, MBP-62, MBP-63, MBP-72, and MBP-76) expressing partial sequences of xlProminin-1 were generated by inserting PCR-amplified fragments of xlProminin-1 into the pMal-c2X vector (New England BioLabs, Beverly, MA), which attaches a maltose binding protein (MBP) tag to the N terminus of the expressed protein. A 6X His tag was also inserted at the C terminus of the fusion proteins (see Supplementary Fig. S6, http://www.iovs.org/lookup/suppl/doi:10.1167/iovs.11-8635/-/DCSupplemental). These double-tagged fusion proteins were sequentially purified with nickel affinity gel (HIS-Select; Sigma, St. Louis, MO) and amylose resin (New England BioLabs), in accordance with the manufacturer's instructions. This two-step, double-tag purification method greatly reduces the copurification of the bacterial histidine or maltose binding proteins, a drawback for both systems if used individually, and ensures the purity and integrity of the purified proteins.[30] The purified proteins were dialyzed against 100 mM sodium phosphate buffer, pH 7.4, and were stored at 4°C, supplemented with sodium azide at a final concentration of 0.05%.

Affinity Purification of Antibodies

Given that GST fusion proteins were used to immunize the rabbits, to avoid purification of anti–GST antibody, we used MBP fusion proteins to affinity purify the antibodies. MBP-PN was used to purify the anti-xlProminin-1 N terminus antibody αPN and MBP-72 was used to purify the anti-xlProminin-1 C terminus antibody αPC. Three micrograms of purified MBP-PN or MBP-72 was coupled to 5 mL activated affinity chromatography media (Affi-Gel 15; Bio-Rad, Hercules, CA), and columns were prepared according to manufacturer's protocol. Immunoglobulins from antisera were first precipitated with 31.8% ammonium sulfate, resolubilized, and dialyzed against 100 mM sodium phosphate buffer, pH 7.4. This material was passed through the MBP fusion protein-coupled gel column. The column was washed with RIA-E buffer (100 mM sodium phosphate buffer, pH 7.6, 0.1% Triton X-100), and antibodies binding to the gel were eluted with an acidic solution containing 0.1 M NaCl and 0.2 M glycine-HCl, pH 2.3. Eluted antibodies were immediately neutralized with 3 M Tris-HCl, pH 8.0, dialyzed against 100 mM sodium phosphate buffer, pH 7.4, and were stored at

Table 1. Sequences of Polypeptides Fused to the C Terminus of GST for Generation of αPN and αPC Antibodies

	Sequences
PN	GYVPAESYETDAYHEPGAIGLLFHIVQGFLYIVQPNAFPQDLVRKVAQQKFGEIRN
PC	LAKFYRRMDTEDVYDDATEQW

4°C with a supplement of sodium azide to a final concentration of 0.05%.

Peptide Competition Assays to Verify the Specificity of Antibodies

Affinity-purified antibody αPN or αPC was preincubated with one of the purified proteins (MBP, MBP-PN, MBP-612, MBP-62, MBP-63, MBP-72, MBP-76) or one of the synthetic peptides (PR [LAKFYRRMDTEDVYDDATEQW], containing the αPC epitope, or PK [MSSYDTVNRFPRASAPPRQDD], containing neither the αPC nor the αPN epitope) before they were used in immunoblotting and immunohistochemistry. Two micrograms of primary antibody (αPN or αPC) was added to a Tris-buffered solution (pH 7.4) containing 10 μg fusion protein or 5 μg synthetic peptide PR or PK. The mixture was incubated at 4°C overnight on a rotator to allow efficient binding of antibody and antigen. The mixture was briefly centrifuged, and the supernatant was used in immunoblotting and immunohistochemistry experiments.

Immunoprecipitation Assay to Verify Specificity of Antibodies

Two eyes from a *X. laevis* tadpole were homogenized in radioimmunoprecipitation assay (RIPA) buffer,[31] followed by incubation with antibody αPN at 4°C overnight with rotation. Protein A agarose beads (Thermo Scientific, Waltham, MA) were added to the mixture, followed by incubation at room temperature for 1 hour. Beads were pelleted by centrifugation (IP), and the depleted supernatant (DS) was transferred to a different tube. Pelleted beads were washed with RIPA buffer 3 times. Laemmli loading buffer was added to the IP and the DS fractions and boiled for 3 minutes. Proteins from the IP and DS fractions were separated on an SDS-PAGE gel by electrophoresis, transferred to a polyvinylidene difluoride (PVDF) membrane, and probed with antibody αPC. Alternatively, the SDS-PAGE gel was stained with silver.

Fractionation of Retinal Membrane Proteins

Retina membrane fractionation was performed in accordance with procedures developed by Papermaster et al.[32] Retinas from dark-adapted adult frogs were isolated under dim red light, suspended in 1.15 g/mL sucrose solution, and gently triturated with an 18-gauge trocar for 10 passages to shear off the outer segments at the connecting cilium, overlaid with 1.10 g/mL sucrose, and centrifuged at 30,000*g* in a rotor (JA-20; Beckman Coulter, Hiahleah, FL) for 20 minutes at 4°C. Membranes floating between the 1.10 and 1.15 g/mL interface, which contained the ROS and COS, were isolated by aspiration and designated the OS fraction. The pellet was resuspended in 0.25 M sucrose, homogenized in a loose-fitting Teflon (DuPont)-glass homogenizer with eight passages and, centrifuged at 1000*g* for 4 minutes at 4°C. The pellet from this centrifugation contained the nuclei and large fragments of less disrupted cell compartments. The supernatant was centrifuged at 200,000*g* in a rotor (SW 40 Ti; Beckman Coulter) for 40 minutes at 4°C; the pellet from this centrifugation was resuspended in 10 mM Tris-acetate, pH 7.4. This "postnuclear fraction" was designated the intermediate fraction (IF) and contained heterogeneous membranes from rod and cone IS and other retinal cell types. Phenylmethylsulfonyl fluoride (0.1 mM) and a protease inhibitor cocktail (Sigma) were added to all sucrose solutions before homogenization. All sample handling procedures were performed on ice. Protein concentrations were measured with a bicinchoninic acid based assay (BCA Protein Assay Kit; Pierce, Rockford, IL) and with BSA (2.00–0.01 mg/mL) as standard.

Preparation of Membrane Proteins from Brain, Kidney, and Testis

We followed the procedure of Corbeil et al.[33] with slight modifications to prepare the membrane proteins. *X. laevis* tissues were homogenized at 4°C in 300 mM sucrose, 5 mM EDTA, 10 mM Hepes-KOH, pH 7.5, supplemented with protease inhibitor mix (Sigma), and centrifuged at 1000*g* for 10 minutes. The supernatant was centrifuged at 40,000*g* for 30 minutes, and the membrane pellet was resuspended in 1% SDS, 20 mM sodium phosphate, pH 7.5. This material was then used for analysis by deglycosylation and immunoblotting.

Immunoblotting of Proteins from *X. laevis* Photoreceptors with Antibodies

Thirty micrograms of protein from the sucrose gradient fractions was mixed with an equal volume of 2× Laemmli loading buffer,[34] boiled for 3 minutes, and loaded into each well of a precast 4% to 15% acrylamide gradient gel (Bio-Rad). Separated proteins were electrophoretically transferred to a PVDF membrane (Millipore, Billerica, MA) and blocked with 5% nonfat powdered milk (Carnation Milk Co., Vevey, Switzerland). Primary antibody incubation was performed at 4°C overnight. PVDF membranes were washed with 1× Tris-buffered saline with 1% Tween-20 (TBST) and incubated with secondary goat anti–rabbit IgG antibodies conjugated with horseradish peroxidase (Fisher Scientific, Pittsburgh, PA) at room temperature for 2 hours. Acetylated α-tubulin, detected by anti–acetylated α-tubulin antibody (Sigma; produced in mouse clone 6–11B-1, ascites fluid) was used as an internal loading control. Chemiluminescence reagent (Western Lightning Chemiluminescence Reagent Plus; PerkinElmer, Waltham, MA) was used for signal detection.

Immunohistochemistry of Photoreceptors with Antibodies

X. laevis tadpoles (at developmental stages 50–55) were euthanized at different time points in the same environment in which they were entrained. Dim red light was used to facilitate the procedure if the tadpoles were euthanized at dark. Excised eyes were fixed in 4% paraformaldehyde in phosphate-buffered saline (PBS), pH 7.4, at 4°C for 1 hour and embedded in OCT (Ted Pella, Inc., Redding, CA) for cryosectioning. Sections (12 μm in thickness) were washed with PBS and treated with 6 M guanidine hydrochloride for 10 minutes to enhance labeling.[35] For double-immunolabeling procedures, sections were incubated with a mixture of two different primary antibodies (final concentration, 2 μg/mL each) overnight at room temperature, washed with PBS, and incubated with a mixture of two secondary antibodies conjugated with fluorescent dyes (final concentration, 2 μg/mL each) for 4 hours at room temperature. Secondary antibodies used in this study were as follows: Alexa Fluor 488 goat anti–rabbit IgG (H+L; Invitrogen) and Texas Red-X goat anti–mouse IgG (H+L; Invitrogen). After labeling with the antibodies, the sections were washed in PBS, incubated with Hoechst 33342 dye (Invitrogen) at a concentration of 10 μg/mL to visualize the nuclei, washed again in PBS, and mounted in mounting medium (Mowiol; Calbiochem, Temecula, CA). Immunolabeling of murine retina was performed in a similar fashion. Confocal images were obtained using a laser scanning microscope (510 LSM; Zeiss, Oberkochen, Germany) at the Center for Cell Analysis and Modeling, University of Connecticut Health Center.

Electron Microscopy

X. laevis eyes were fixed in 4% paraformaldehyde (Electron Microscopy Science, Hatfield, PA) in 0.25 M Hepes, pH 7.4, at 4°C for 1 hour. Retinas embedded in LR White or LR Gold were unreactive with the antibodies. Therefore, fixed retinas were dissected, embedded in 10% gelatin, and infiltrated with 2.3 M sucrose. Tissues were frozen by plunging into liquid nitrogen, and ultrathin cryosections were cut with a cryo ultramicrotome (EM FC6/UC6; Leica, Wetzlar, Germany), blocked with 1% BSA in PBS and incubated in primary antibodies (αPN or αPC; final concentration, 2 μg/mL) overnight, and subsequently stained with secondary antibody goat anti–rabbit IgG (H+L; final concentration, 2 μg/mL; Invitrogen) and protein A 6 nm gold (Electron Microscopy Science). Sections were postfixed with 1% glutaraldehyde in PBS, counterstained with 2% neutral uranyl acetate, and observed under a transmission electron microscope (JOEL 100CX; Tokyo, Japan) at the Center for Cell and Molecular Imaging at the Yale University School of Medicine.

Construction of Plasmid Vectors That Drive Expression of the Transgenes in *X. laevis* Rods or Cones

All expression vectors are based on pEGFP-N1 obtained from Clontech Laboratories, Inc. For transgene expression in *X. laevis* rods, the vector was modified to contain the *X. laevis* opsin promoter (XOP1.3) in place of the CMV promoter, as described previously.[36] The coding sequence of eGFP in the original pEGFP-N1 vector was replaced with that of hrGFP II (Stratagene), and five unique restriction sites (*Fse*I, *Asc*I, *Not*I, *Sca*I, and *Eco*RV) were introduced to the 5′ end of the promoter. This modified vector was named FANSE-XOP1.3-hrGFP II N1. A vector for cone specific expression, FAN-XtCAP1.9-hrGFP II N1, was constructed by replacing the XOP1.3 promoter in the FANSE-XOP1.3-hrGFP II N1 vector with a 1.9-kbp genomic sequence obtained with PCR from the 5′ end of the *X. tropicalis* cone arrestin (*ARR3*) gene, including partial sequence of the first exon (see Supplementary Fig. S7 for the sequence of the XtCAP1.9 promoter and Supplementary Fig. S8 for a map of the FAN-XtCAP1.9-hrGFP II N1 vector [both figures available at http://www.iovs.org/lookup/suppl/doi:10.1167/iovs.11-8635/-/DCSupplemental]). Primers used for amplifying the 1.9-kbp genomic sequence at the 5′ end of the *X. tropicalis* cone arrestin (*ARR3*) gene are 5′-ATAAGAATGCGGCCGCGAAGCTTGAGGAGGACTACCCC-3′ and 5′-CGCAGATCTTACCTGTATCAGTTCTCTTGGACTTCAG-3′.

The two blunt end restriction sites, *Sca*I and *Eco*RV, were lost in the resultant vector during the construction procedure. The constructed FAN-XtCAP1.9-hrGFP II N1 vector was tested for its ability to drive expression of hrGFP II specifically in cone photoreceptors of transgenic *X. laevis* tadpoles (see Supplementary Fig. S9, http://www.iovs.org/lookup/suppl/doi:10.1167/iovs.11-8635/-/DCSupplemental).

Expression of Prominin-1-hrGFP II in Transgenic *X. laevis* Photoreceptors

X. laevis prominin-1 cDNA was amplified by PCR using primer pairs that incorporate *Kpn*I and *Bam*HI sites on the ends of its open reading frame (ORF). A Kozak consensus sequence[37] (−6 GCCACCATGG +4) was introduced in front of the ORF to enhance the expression of the transgene in eukaryotic cells (see Supplementary Fig. S10 for the diagram and sequence of the fusion protein, http://www.iovs.org/lookup/suppl/doi:10.1167/iovs.11-8635/-/DCSupplemental). Amplified PCR fragments were cloned into either the FANSE-XOP1.3-hrGFP II N1 or the FAN-XtCAP 1.9-hrGFP II N1 expression vector for expression of the transgene in rods or cones, respectively. Plasmids containing the xlProminin-1-hrGFP II expression cassette were linearized with restriction endonuclease *Not*I, mixed with the permeabilized sperm nuclei, and injected into *X. laevis* eggs, as described by Kroll and Amaya,[38] with modifications described by Moritz et al.[36] Transgenic tadpoles expressing the transgene were screened using a dissection microscope (MZ8; Leica) equipped for hrGFP II fluorescence detection.

Results

Detection of xlProminin-1 in Membrane Fractions of *X. laevis* Retina, Brain, and Kidney by Immunoblotting

We generated rabbit polyclonal antibodies αPN and αPC, specific to the N and C termini of xlProminin-1, respectively, using purified GST fusion proteins expressed in *E. coli* as immunizing antigens. Specificities of both antibodies were verified by antigen competition assays (see Supplementary Figs. S1, S2, and Supplementary Table S1, all available at http://www.iovs.org/lookup/suppl/doi:10.1167/iovs.11-8635/-/DCSupplemental) and immunoprecipitation of xlProminin-1 protein from *X. laevis* eyes (see Supplementary Fig. S3, http://www.iovs.org/lookup/suppl/doi:10.1167/iovs.11-8635/-/DCSupplemental). Membrane proteins from the *X. laevis* retina were fractionated into outer segments (OS) and intermediate fractions (IF) by sucrose density gradient centrifugation and analyzed by immunoblotting. The OS fraction contains both ROS and COS. The IF contains a mixture of membranes of the retina after removal of ROS, COS and nuclei.[39] Membrane proteins extracted from brain and kidney were also analyzed. Both αPN and αPC detect a protein of approximately 95 kDa in both OS and IF fractions of the retina (Fig. 1, filled arrows). This protein likely represents full-length xlProminin-1. Peptide: N-glycosidase F (PNGase F) treatment reduced the molecular weight of this protein to approximately 80 kDa. A minor band of approximately 45 kDa was detected with αPN, but not with αPC, in the retina IF (Fig. 1, hollow arrow) and was the predominant band detected in membrane proteins from brain and kidney. The size of this minor band was reduced to approximately 30 kDa after PNGase F treatment. No full-length (95 kDa) xlProminin-1 product was detected by either αPN or αPC in the brain or kidney membrane protein extracts. A low

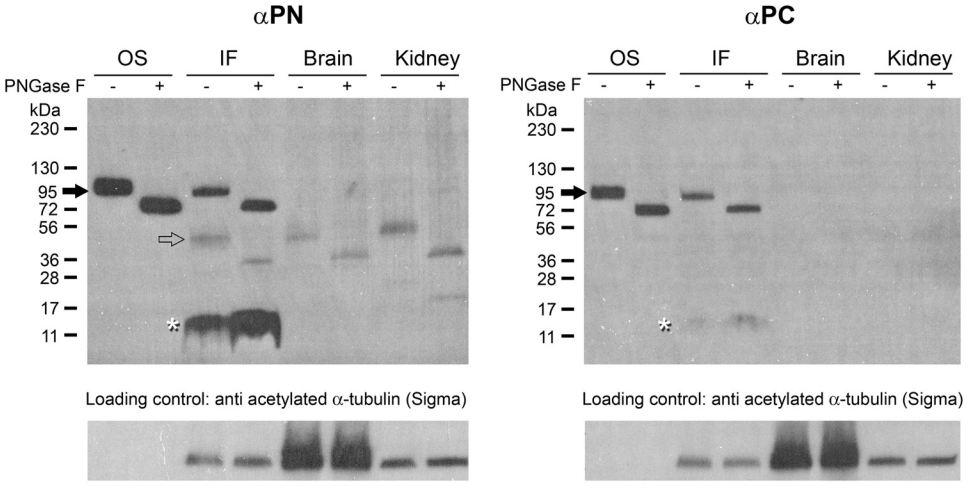

Figure 1. Detection of xlProminin-1 in membrane fractions of *X. laevis* retina, brain, and kidney by immunoblotting. Membrane proteins extracted from *X. laevis* retina OS, IF, and from brain and kidney were immunoblotted with either anti–xlProminin-1 N terminus antibody αPN or anti–xlProminin-1 C terminus antibody αPC for the presence of xlProminin-1 protein. A product of approximately 95 kDa was detected in OS and IF fractions of the retina by both αPN and αPC antibodies (*filled arrows*). PNGase F treatment reduced the molecular weight of this protein to approximately 80 kDa. This product may represent full-length xlProminin-1. No 95-kDa product is detected with either αPN or αPC in membrane proteins extracted from the brain or kidney. A minor band (approximately 45 kDa, *hollow arrow*) was detected by αPN antibody in the IF fraction of the retina, and the membrane protein from brain and kidney. The molecular weight of this protein was reduced to approximately 30 kDa after PNGase F treatment. A low molecular band (*asterisk*) detected by both αPN and αPC in the IF fraction of retina may represent the degradation products of xlProminin-1 because this band contains epitopes from both N and C termini of xlProminin-1, but with a much lower molecular weight (approximately 12 kDa) than that of the full-length protein. Anti–acetylated α-tubulin antibody was used as a loading control.

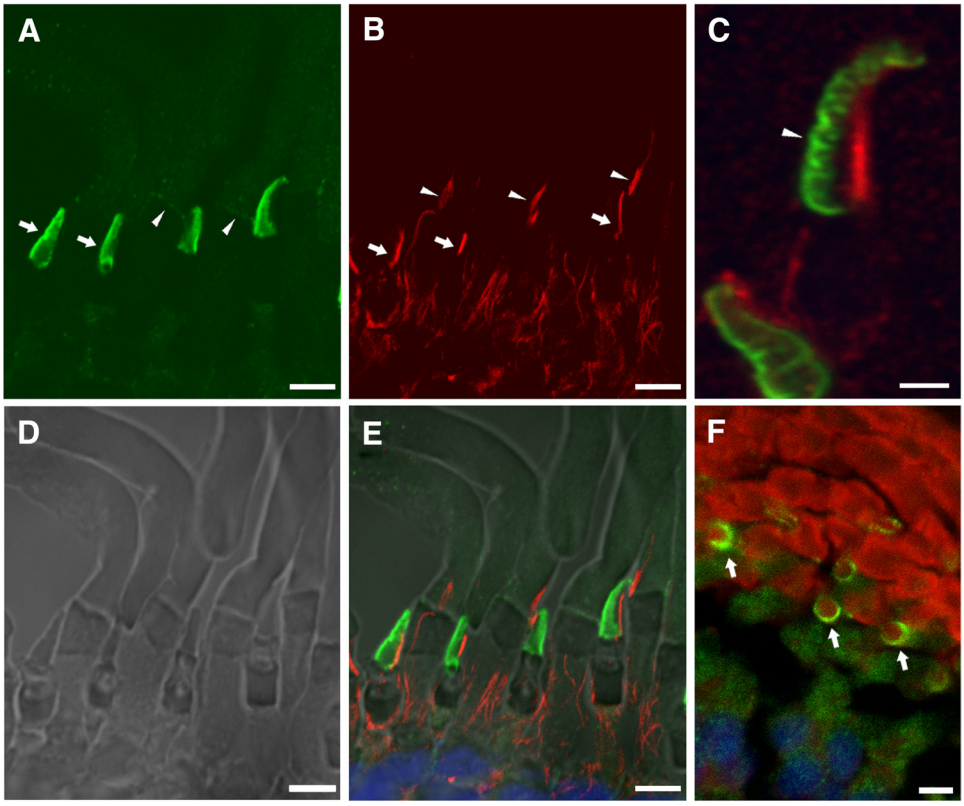

FIGURE 2. Double immunolabeling of *X. laevis* photoreceptors with anti–xlProminin-1 N terminus antibody αPN and anti–α-tubulin antibody. Sections of *X. laevis* retina were double immunolabeled with αPN and anti–acetylated α-tubulin antibody. (**A**) The COS is brightly labeled with αPN (*green*) predominantly on one side (*arrows*). The base of the ROS is also faintly labeled with αPN as a thin band (*arrowheads*). Distal ROS is diffusively labeled with αPN at low intensity. The labeling intensity of αPN on COS is much greater than on ROS. (**B**) The same section of retina was labeled with anti–acetylated α-tubulin antibody (*red*). Axonemes of the connecting cilia of both rods (*arrowheads*) and cones (*arrows*) are labeled with that antibody. (**C**) A longitudinally sectioned cone cell on the upper part of the image shows clearly separated labeling of xlProminin-1 and α-tubulin. Labeling of αPN on the rims is confined to one side of the COS (*arrowhead*). A differently oriented cell is also seen on the *lower left*. (**D**) Nomarski view of the same retina section to show the morphology of cells. (**E**) Superimposed image to show the relative position of αPN and anti–α-tubulin immunolabeling. αPN labels the lamellar rims opposite the axoneme of the COS. (**F**) Cross-section of a tadpole retina labeled with αPN (*green*) and Texas Red-X conjugated wheat germ agglutinin (*red*) that binds to glycosylated photopigments. The semicircular pattern of αPN labeling is readily seen in the cross-sectioned COS (*arrows*), further demonstrating the asymmetrical distribution of xlProminin-1 in this organelle. Scale bars: 2 μm (**A**, **B**, **D**, **E**); 5 μm (**C**, **F**).

molecular band that may represent a degradation product of xlProminin-1 was detected with both αPN and αPC in the IF of the *X. laevis* retina (Fig. 1, asterisks). These results suggest that xlProminin-1 is proteolyzed in retina, brain, and kidney but remains intact in both COS and ROS.

xlProminin-1 Resides on Cone Lamellae in a Domain Opposite the Connecting Cilium Axoneme

The connecting cilium is nonmotile (9+0) and filled with microtubules that partially radiate into the OS beyond its base.[2] It readily labels with antibody to acetylated α-tubulin (Fig. 2B). Double labeling of sections of the *X. laevis* retina with αPN and anti–acetylated α-tubulin revealed the presence of xlProminin-1 on the outer rims of the cone lamellae, on the side opposite the cilium (Figs. 2C, 2E). Cross-sections revealed a semicircle of anti–xlProminin-1 labeling on one side of the COS lamellar rim (Fig. 2F). αPC also asymmetrically labeled the rims of COS (Fig. 3) in a pattern that was essentially indistinguishable from that observed with αPN. Because antibodies to both the N and C termini of xlProminin-1 label the same domains of COS and the immunoblotting results indicate the presence of uncleaved xlProminin-1, we interpret these results to indicate the localization of the full-length protein at this site in the membrane of COS.

xlProminin-1 and Peripherin-2/rds Reside in Mutually Exclusive Domains of COS Lamellae

Double immunolabeling of cones with either αPN or αPC and anti–peripherin-2/rds monoclonal antibody Xper5A11 (a gift from Robert S Molday, University of British Columbia) produced similar results: xlProminin-1 and peripherin-2/rds reside in mutually exclusive domains of COS lamellae (Figs. 4, 5). Previous studies have shown that peripherin-2/rds localizes specifically to the closed rim of the COS lamellae, a domain homologous to the closed disk rim of ROS and adjacent to the axoneme.[40,41] By contrast, xlProminin-1 localizes to the open lamellar rim opposite the axoneme.

xlProminin-1 Localizes to the Basal and Distal Membranes of ROS

The intensity of immunolabeling of ROS with both anti-xlProminin-1 antibodies appeared much weaker than that of COS. Moreover, the labeling of ROS with both anti-xlProminin-1 antibodies varied greatly throughout different phases of the light cycle and between individual animals. Antibodies αPN and αPC both label the base of the ROS as a thin band in some, but not all, 12-hour light/12-hour dark cycled animals (Figs. 2A, 4B for αPN; Figs. 3B, 5A for αPC). For example, immunolabeling of αPN at the base of the ROS in a tadpole euthanized 4 hours before light onset (Figs. 6A, 6B) is compared with that of a littermate euthanized 8 hours after light onset (Figs. 6C, 6D). Clearly visible but faint labeling of xlProminin-1 at the base of the ROS is seen in the tadpoles euthanized at the late stage of the light phase, whereas xlProminin-1 is not detectable at the base of the ROS in retinas of tadpoles euthanized in the dark phase. Immunolabeling of xlProminin-1 at the base of the ROS with αPC revealed results similar to those seen with αPN (data not shown). By contrast, the high intensity of COS labeling with either of the antibodies was constant throughout the light cycle. Antibodies αPN and αPC both also faintly labeled

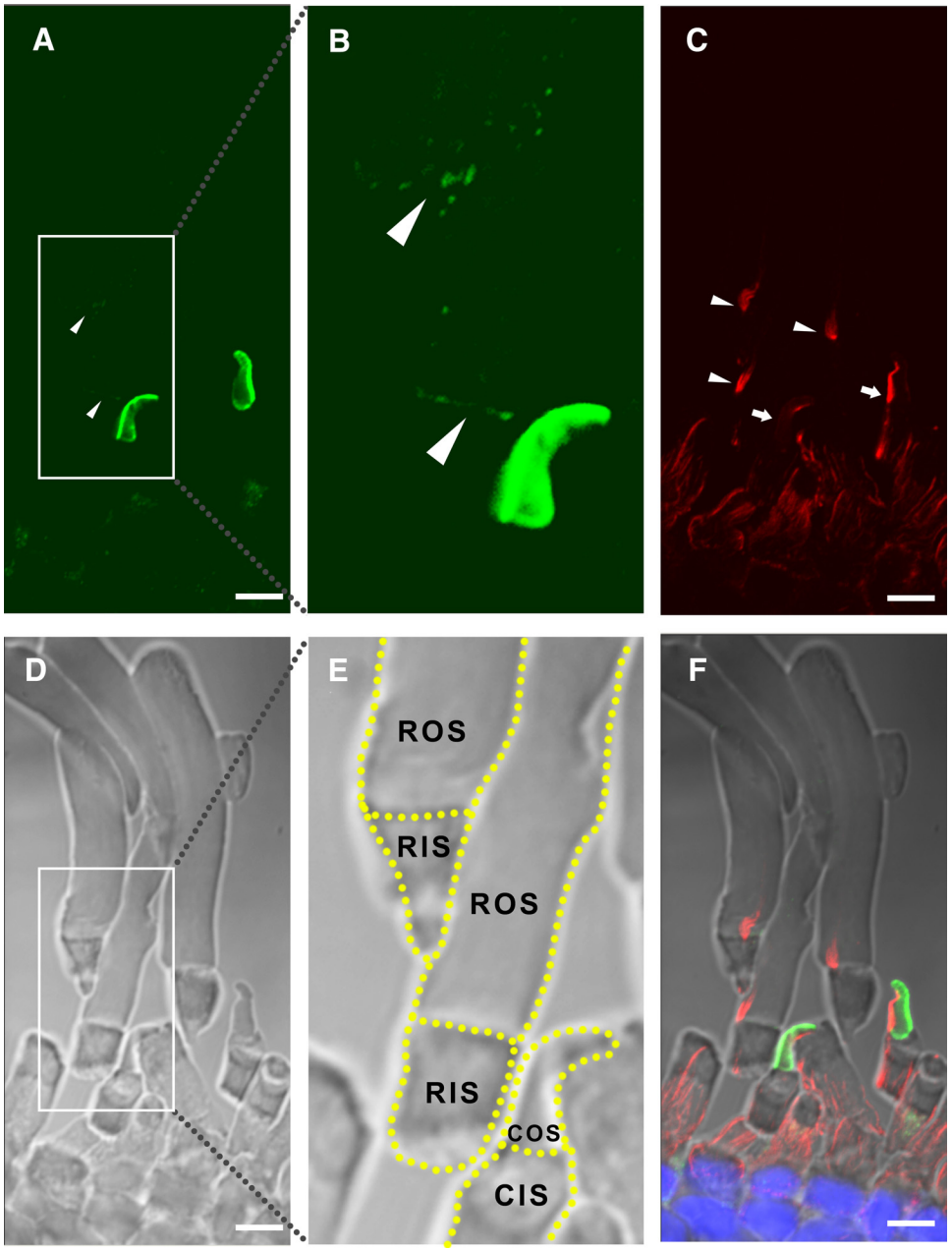

FIGURE 3. Double immunolabeling of *X. laevis* photoreceptors with anti–xlProminin-1 C terminus antibody αPC and anti–α-tubulin antibody. (**A**) The COS is brightly labeled with αPC (*green*) predominantly on one side. The base of a ROS (*arrowheads*) is also labeled with αPC as a thin faint band. Distal ROS is diffusively labeled by αPC, as it is by αPN (Fig. 2). (**B**) Enlarged, brightened, and contrast-enhanced images of *boxed areas* in (**A**) to show the basal labeling of ROS (*arrowheads*). (**C**) The same retina section was labeled with anti–acetylated α-tubulin antibody (*red*). Axonemes of the connecting cilia of both rods (*arrowheads*) and cones (*arrows*) are labeled. The antibody also labels the filaments that extend from the calycal processes into the inner segment to the level of the external limiting membrane. (**D**) Nomarski view of the same retina section to show the morphology of cells. (**E**) Nomarski view of the same enlarged area as in (**B**). Contours of individual photoreceptors are marked with *dashed lined*. (**F**) Superimposed image to show the relative position of αPC and anti–α tubulin immunolabeling. αPC labels the lamellar rims opposite to the axoneme of the COS. CIS, cone inner segment; RIS, rod inner segment. Scale bar, 5 μm.

the entire ROS in a diffuse pattern, which was only slightly greater than background labeling (Figs. 2A, 4B for αPN; Figs. 3B, 5A for αPC).

Detection of xlProminin-1 in *X. laevis* Photoreceptors by Immunoelectron Microscopy

To study xlProminin-1 localization in photoreceptors with high resolution, we performed immunoelectron microscopy with xlProminin-1 antibodies on thin sections of retinas embedded by rapid freezing after infiltration with sucrose. We turned to this approach because sections of retinas embedded in a variety of hydrophilic plastics failed to label with our antibodies. Retinas of *X. laevis* tadpoles were cryosectioned and subject to reaction with αPN and αPC antibodies, which were then detected by anti–rabbit IgG antibodies and protein A-gold conjugates. Immunoelectron microscopy showed the same localization pattern of xlProminin-1 in COS. Both antibodies labeled only the rims of COS lamellae opposite the connecting cilium. Rims on the side of the connecting cilium and the interior disk membrane were not labeled above background (Figs. 7A, 7B for COS labeling with αPN; Fig. 8A for COS labeling with αPC).

αPN labeled the whole ROS at low density compared with the uniform dense labeling observed with anti-opsin antibody.[42] Rod IS (RIS) were only sparsely labeled with αPN (Fig. 7C). All these observations are in accordance with our studies conducted with fluorescence immunohistochemistry. This intra-diskal labeling of distal ROS disks by αPN is specific because the labeling was confined to the ROS, blocked by competition with MBP fusion protein antigens (data not shown), and did not label interphotoreceptor spaces or RPE cells.

The labeling density of αPN at the base of the ROS was not higher than the remaining part of the more distal portions, in contrast to the observation made with the same antibody in immunofluorescence studies, in which αPN labeled the base of ROS as a faint thin band (Figs. 2A, 4B), especially if the tadpoles were euthanized at the late stage of the light phase (Figs. 6C, 6D).

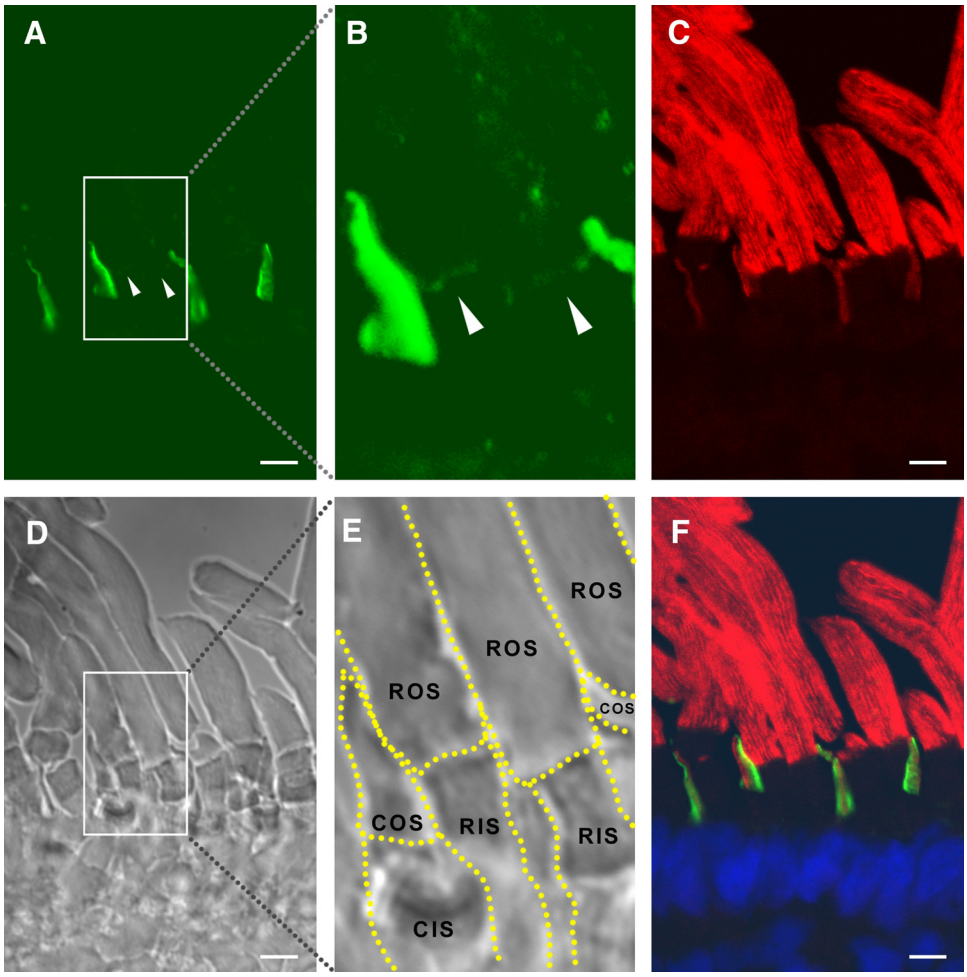

FIGURE 4. Double immunolabeling of *X. laevis* photoreceptors with anti–xlProminin-1 N terminus antibody αPN and anti–peripherin-2/rds antibody Xper5A11. (**A**) The COS is brightly labeled asymmetrically with αPN (*green*). The base of the ROS is labeled with αPN as a thin, faint band (*arrowheads*). (**B**) Enlarged, brightened, and contrast-enhanced images of boxed areas in (**A**) to show the basal labeling of ROS (*arrowheads*). (**C**) The same retina section was labeled with anti–peripherin2/rds antibody Xper5A11 (*red*). Both COS and ROS are labeled with Xper5A11, but the COS labeling is confined to a thin area along the length of one side of the COS, whereas the ROS are labeled circumferentially except for the interiors of the incisures, which are viewed as parallel unlabeled longitudinal lines. (**D**) Nomarski image of the same retina section to show the morphology of cells. (**E**) Nomarski view of the same enlarged area as in (**B**). Contours of individual photoreceptors are marked with *dashed lines*. (**F**) Superimposed image to show the relative position of αPN and Xper5A11 immunolabeling. αPN labels the lamellar rims opposite the side that is labeled with Xper5A11 on the COS. The thin band labeled with αPN at the base of ROS does not overlap with the Xper5A11 labeling of the mature disks above. Scale bar, 5 μm.

This difference between fluorescence and electron microscopic immunolabeling could be explained if xlProminin-1 were localized only to the rims of the large basal ROS lamellae of frogs but not to the interior of the growing disk membranes. In this scenario, only fortuitous sections along the rim of the growing disk would reveal xlProminin-1 at high density, when ultrathin sections of frog rods were cut. αPC did not label, or only sparsely labeled, ROS and RIS in frozen thin sections (Fig. 8B).

Localization of xlProminin-1-hrGFP II Fusion Protein in Rods and Cones of Transgenic *X. laevis*

To evaluate xlProminin-1 distribution by an independent method and to test a possible position for fluorescence tagging the molecule, we generated transgenic *X. laevis* tadpoles expressing xlProminin-1-hrGFP II fusion protein in either rod or cone photoreceptors, driven by the *X. laevis* opsin promoter XOP1.3[36] or the *X. tropicalis* cone arrestin promoter XtCAP1.9, respectively. See Supplementary Figure S7 for the sequence of XtCAP1.9 promoter and Supplementary Figure S9 for its specific promoter activity in cones (both figures available at http://www.iovs.org/lookup/suppl/doi:10.1167/iovs.11-8635/-/DCSupplemental). Splice variant s2 of xlProminin-1 (3a−, 8a−, 11a+, 19a+, 26b−, 27−, 28a−) was used in generating the fusion protein, because xlProminin-1, lacking alternative exons 26b, 27, and 28a, represents one of the predominant forms of the mRNA in *X. laevis* retina, as shown by RT-PCR results.[29] The predicted full sequence of the fusion protein is given in Supplementary Fig. S10 (http://www.iovs.org/lookup/suppl/doi:10.1167/iovs.11-8635/-/DCSupplemental).

The xlProminin-1-hrGFP II fusion protein localized to the rims of the open lamellae in COS, opposite the domain immunolabeled by anti–peripherin-2/rds, and the same location at which the endogenous xlProminin-1 was detected by antibodies (Figs. 9A–D). The localization pattern of xlProminin-1-hrGFP II in rods, however, did not always correlate well with the localization pattern of the endogenous protein observed by immunocytochemistry. The fusion protein was localized to the plasma membrane of both the RIS and the ROS and occasionally intercalated into the inner ROS (Figs. 9E, 9F). The base of the ROS was occasionally labeled (Figs. 9G, 9H), a result that paralleled our immunocytochemical study results. This mislocalization of xlProminin-1-hrGFP II in rods might have been caused by the saturation of xlProminin-1 localization sites by introducing large amounts of exogenous fusion proteins. Moreover, we observed distortion and deformation of the ROS in rods expressing high levels of the xlProminin-1-hrGFP II fusion protein, suggesting that saturation of xlProminin-1 localization sites may cause a ROS structural defect. The variable levels of transgene expression are probably caused by positional effect variegation given that expression units are randomly inserted into the genome of the animal.[43]

DISCUSSION

The process of disk morphogenesis and maturation in rods and cones is becoming clarified as several proteins have been proposed to participate in this process, including peripherin-2/rds and rom-1, which are specifically localized to the OS disk rims.[44,45] Prominin-1 has drawn attention because of its strategic localization at the basal disks of murine rods first reported by Maw et

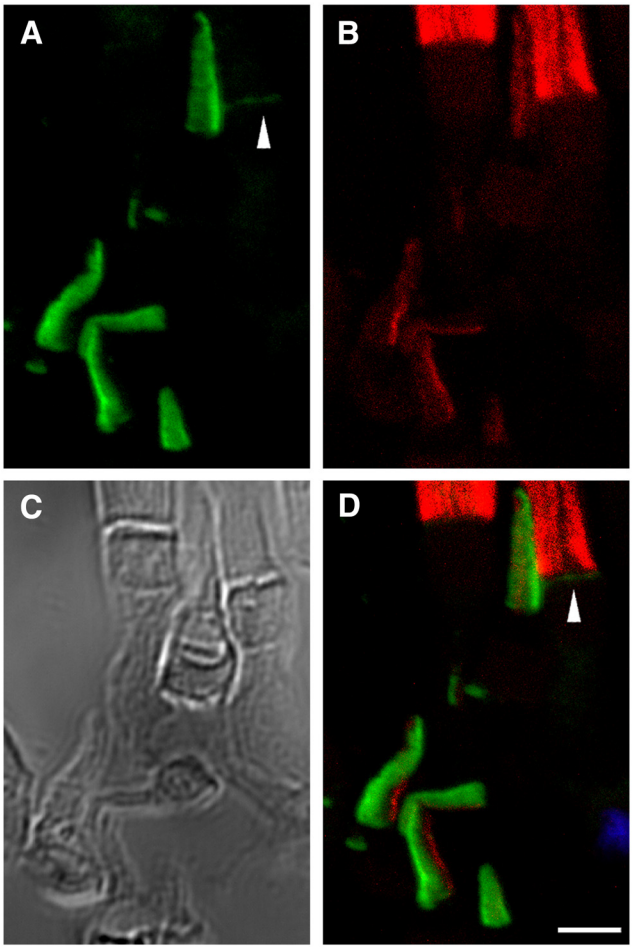

FIGURE 5. Double immunolabeling of *X. laevis* photoreceptors with anti–xlProminin-1 C terminus antibody αPC and anti–peripherin-2/rds antibody Xper5A11. (**A**) COS is brightly labeled asymmetrically with αPC (*green*). The base of the ROS is labeled with αPC as a thin faint band (*arrowhead*). (**B**) The same retina section was labeled with anti–peripherin2/rds Xper5A11 (*red*). Both COS and ROS are labeled with Xper5A11, but the COS labeling is confined to a thin area along the length of one side of the COS, whereas the ROS are labeled circumferentially. Unlabeled longitudinal lines in the ROS are the interiors of the incisures. (**C**) Nomarski view of the same retina section to show the morphology of cells. (**D**) Superimposed image to show the relative position of αPC and Xper5A11 immunolabeling. αPC labels the lamellar rims opposite the side that is labeled with Xper5A11 on the COS. αPC labeling at the base of ROS does not overlap with Xper5A11 labeling (*arrowhead*). Scale bars, 5 μm.

al.[24] and for its contribution to degenerative retinal disorders when it is mutated.[24–26] The presence of prominin-1 at the base of murine cones was revealed by Zacchigna et al.[25] We have now evaluated the expression of xlProminin-1 in *X. laevis* cones and localized it specifically to the open rims of the COS and also confirmed the localization of prominin-1 to the base of murine S and M cones (see Supplementary Figs. S4, S5, http://www.iovs.org/lookup/suppl/doi:10.1167/iovs.11-8635/-/DCSupplemental), where open disks are consistently present. In contrast to frog COS (whose lamellae remain open from the base to the tip), murine COS have a variable degree of separation of their lamellar membranes from the plasma membrane, except for open disks at the base. Rodent COS are composed of closed disks with occasional openings to the extracellular space throughout their length.[46] This may account for the absence of significant prominin-1 labeling on one side of murine COS that contrasts with the pattern seen in the frog COS; if the lamella becomes a closed disc, even transiently, it will, supposedly, have no prominin-1 at its rim.

A diagram of xlProminin-1 and peripherin-2/rds localization in rods and cones of *X. laevis* is presented in Figure 10. The mutually exclusive distribution of xlProminin-1 and peripherin-2/rds in *X. laevis* COS shown here reflects, and could be responsible for, the difference between mature ROS disks and COS lamellae. Peripherin-2/rds has membrane fusogenic activity in vitro.[47–52] *X. laevis* expresses three homologs of the peripherin-2/rds and rom-1 family, namely, xrds38, xrds36, and xrds35.[53] They may help to seal or pinch off the mature disks to separate them from the enveloping plasma membrane. These molecular events underlying disk morphogenesis must be tightly coordinated to mediate the morphogenesis of new disks, including the cleavage of disks by incisures, and to distinguish the morphogenesis of ROS disks from COS lamellae. Prominin-1 may play a role in keeping most of the COS lamellae open in *X. laevis*, possibly serving as an anti-fusogenic factor to counterbalance the fusogenic activity of peripherin-2/rds in the process of disk morphogenesis and maturation, thereby preventing the isolation of the COS lamellae from

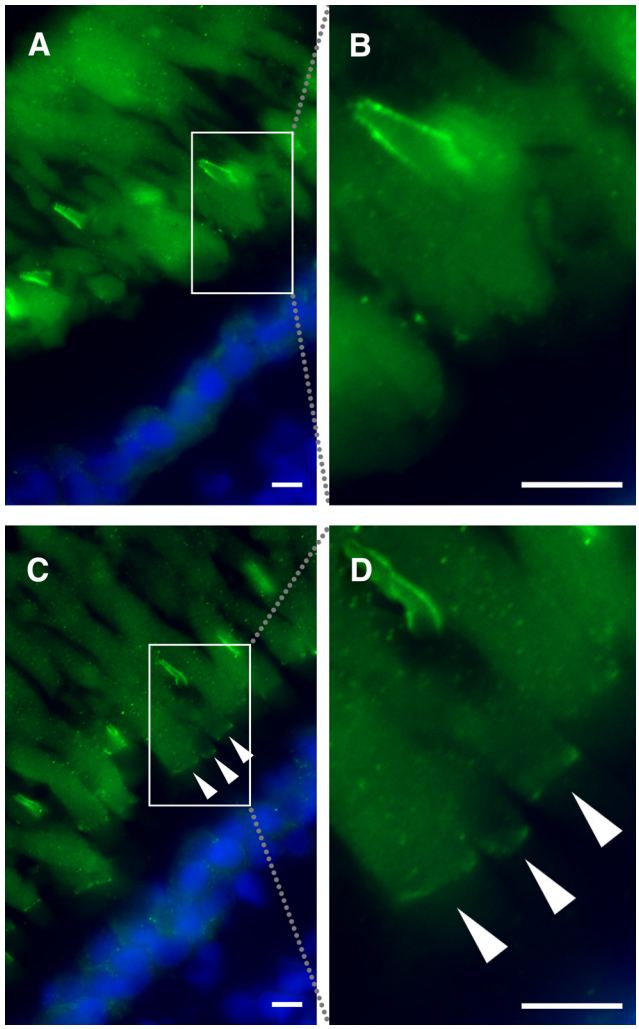

FIGURE 6. Variation in immunolabeling of *X. laevis* rods with anti–xlProminin-1 N terminus antibody αPN. (**A**) Immunolabeling of a retina from a tadpole euthanized at 4 hours before light onset with αPN (*green*). No labeling is seen at the bases of the ROS. The *boxed area* is enlarged as shown in (**B**). (**C**) Immunolabeling of a retina from a tadpole euthanized at 8 hours after light onset with αPN. Bases of the ROS are clearly labeled (*arrowheads*). The *boxed area* is enlarged as shown in (**D**). Nuclei are labeled with Hoechst 33342 dye (*blue*). Scale bars, 5 μm.

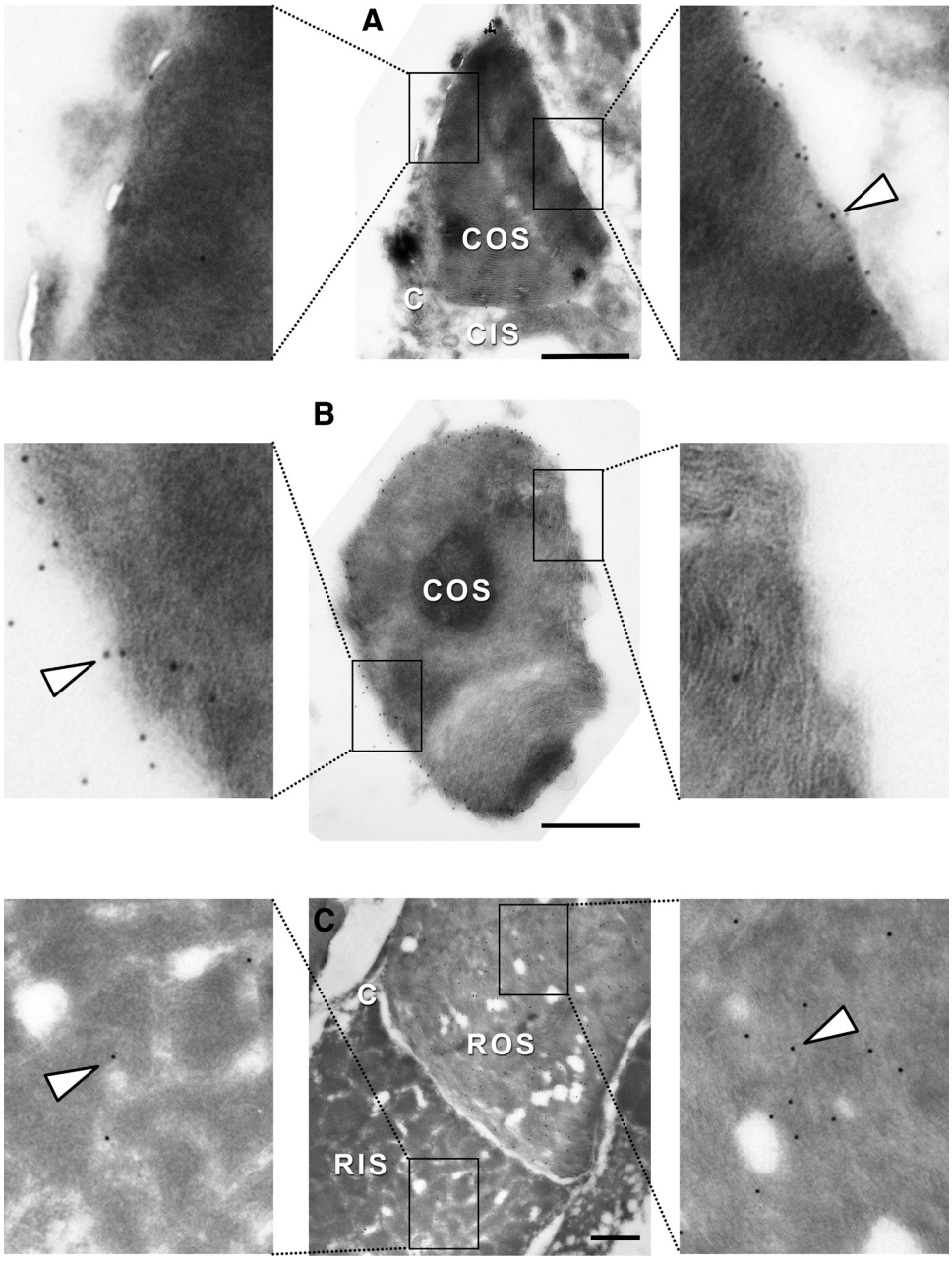

FIGURE 7. Localization of xlProminin-1 with anti–xlProminin-1 N terminus antibody αPN in *X. laevis* photoreceptors examined by immunoelectron microscopy of frozen sucrose-embedded retinas. (**A**) The rims of the disk lamellae of a COS opposite the side of the connecting cilium are labeled with αPN, detected with protein A 6 nm gold (*arrowhead*). Rims of the disk lamellae adjacent to the connecting cilium are not labeled. (**B**) Cross-section of a COS. The entire rim except the right side is labeled with αPN, whereas the interior lamellar membranes are unlabeled. (**C**) Longitudinal section of a rod. The whole ROS is diffusively labeled with αPN at low density. The RIS is only sparsely labeled. Labeling density at the base of this ROS is not higher than at the more distal portions. *Boxed areas* are enlarged fourfold to show details of representative immunolabeling of the sections. The *large holes* are artifacts caused by the instability of the fragile sections. C, connecting cilium. Scale bars, 1 μm.

the plasma membrane. Prominin interacts with spacemaker (spam), a glycoprotein in the interphotoreceptor space in *Drosophila.*[28] It will be of interest to determine whether a comparable interaction occurs in the interphotoreceptor space of vertebrate retinas with an as yet unidentified prominin ligand.

We found that *X. laevis* rods differ significantly from cones in expression and subcellular distribution of xlProminin-1. Antibodies against xlProminin-1 labeled the base of ROS as a faint thin band, and the labeling intensity was considerably less than that observed in the adjacent cones by both immunofluorescence and immunoelectron study, indicating that there is a lower content of xlProminin-1 in the ROS than in the COS. Faint diffuse labeling on the entire length of ROS may reflect trapped xlProminin-1 in closed disks moving toward the distal end of the ROS. Although xlProminin-1 is detected throughout the entire ROS, it does not appear to colocalize with peripherin-2/rds at the base of the ROS, along incisures, or at disk rims of closed disks. (Figs. 3, 5).

The immunolabeling patterns of xlProminin-1 in *X. laevis* ROS are intriguing, because of the variations of the basal labeling of ROS when different animals were observed or when the animals were euthanized at different time points during the light cycle. A thin band at the base of the rods was usually detected in retinas obtained at the later stage (8 hours after light onset) of the light phase in animals kept in a 12-hour light/12-hour dark regimen, as shown in Figures 6C and 6D. Labeling was often undetectable at 2 hours after light offset. If prominin-1 is confined to the open basal lamellae at the base of the ROS, then this finding correlates well with the previous findings by Besharse et al.,[15] who observed that the number of open disks at the base of *X. laevis* ROS varies significantly during the day and night, with the peak number of the open disks (approximately 15) achieved in the mid afternoon. Moreover, a study of *X. laevis* retina produced an image[54] strikingly similar to that observed in our immunolabeling studies of xlProminin-1. By using Lucifer Yellow (a small molecule that

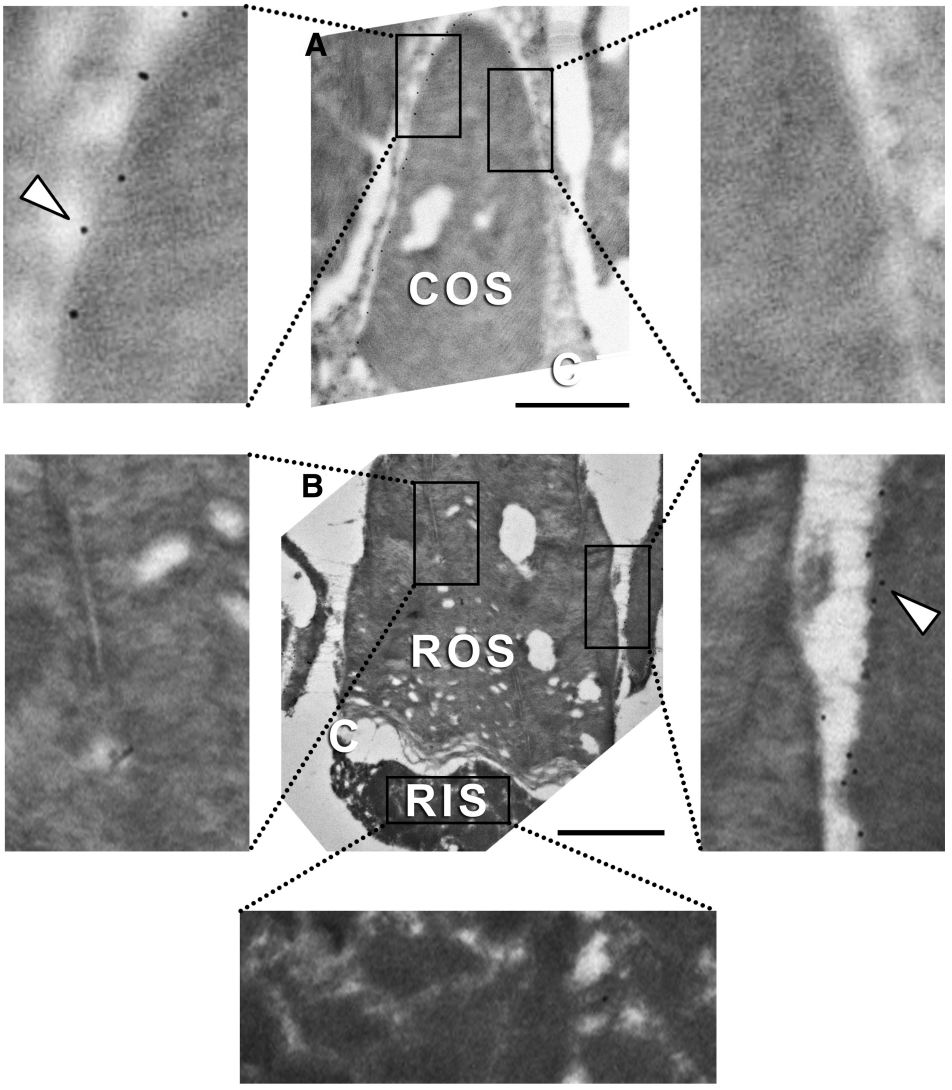

FIGURE 8. Localization of xlProminin-1 with anti–xlProminin-1 C terminus antibody αPC in *X. laevis* photoreceptors examined by immunoelectron microscopy of frozen sucrose embedded retinas. (**A**) The rims of the disk lamellae of a COS opposite the side of the connecting cilium are labeled with αPC, detected with protein A 6 nm gold (*arrowhead*). Rims of the disk lamellae on the same side of the connecting cilium are not labeled. (**B**) Longitudinal section of a rod. ROS and RIS are not labeled with αPC, in contrast to an adjacent labeled COS membrane (*arrowhead*). *Boxed areas* are enlarged fourfold to show the details of typical immunolabeling of the sections. C, connecting cilium. Scale bars, 1 μm.

can penetrate the interlamellar space) to stain the light-adapted *X. laevis* retina, they found that the entire COS, but only the base of ROS and its shedding tip, were stained by penetration of Lucifer Yellow in the extracellular space, showing that these domains are accessible to small molecules in the extracellular compartment. By contrast, COS are always highly labeled, with no obvious circadian or diurnal variation in xlProminin-1 immunolabeling. Although we cannot exclude the possibility that there was indeed circadian or diurnal variation in COS labeling as well, any such variation was below our threshold of detection.

Several important questions arise from these observations: Is the diminishing of immunolabeling at the base of ROS after the peak in late stage of the light phase a consequence of the destruction or recycling of xlProminin-1? Alternatively, are its epitopes masked as the basal lamellae are closed by peripherin-2/rds and rom-1 during disk maturation? Immunoblotting of retinal IF fractions (Fig. 1) reveals that smaller fragments of prominin-1 are readily detected by αPN and, to a lesser extent, by αPC, indicating that the protein has been cleaved. However, the OS fractions contain little, if any, of these fragments (Fig. 1). This result suggests that the low-level labeling in the distal ROS interior comes from the intact xlProminin-1 protein that has been retained after disk closure. xlProminin-1 may be partially transported from the OS to the IS for recycling or for proteolytic degradation. However, because cones were much more intensively labeled than rods with antibodies to xlProminin-1, it is likely that most of the signals in our immunoblotting studies came from xlProminin-1 in cones (Fig. 1) and, therefore, may not reflect prominin-1 dynamics in rods.

Transgenic expression of an xlProminin-1-hrGFP II fusion provided an important support of our immunocytochemcial results in COS. xlProminin-1-hrGFP II localized to the rim of the COS opposite the side containing peripherin-2/rds, the same site where we detected endogenous xlProminin-1 in COS by immunolabeling, thus arguing against epitope masking as a factor influencing our results. The pattern of xlProminin-1-hrGFP II localization in rods, however, was not constant among individual transgenic animals. In addition to the variable labeling at the base of the ROS, the fusion protein was observed along the ROS plasma membrane, with occasional intercalations into the inner ROS, and, in cases of very high expression, into the RIS plasma membrane. Variations of xlProminin-1-hrGFP II localization in rods may reflect the variations of the endogenous xlProminin-1 localization observed with immunolabeling, or they may be artifacts resulting from overexpression relative to the endogenous protein that saturates the capacity of the organelle to house, transport, or organize the protein. This may also contribute to the abnormal shape of ROS observed in retinas expressing high levels of the fusion protein.

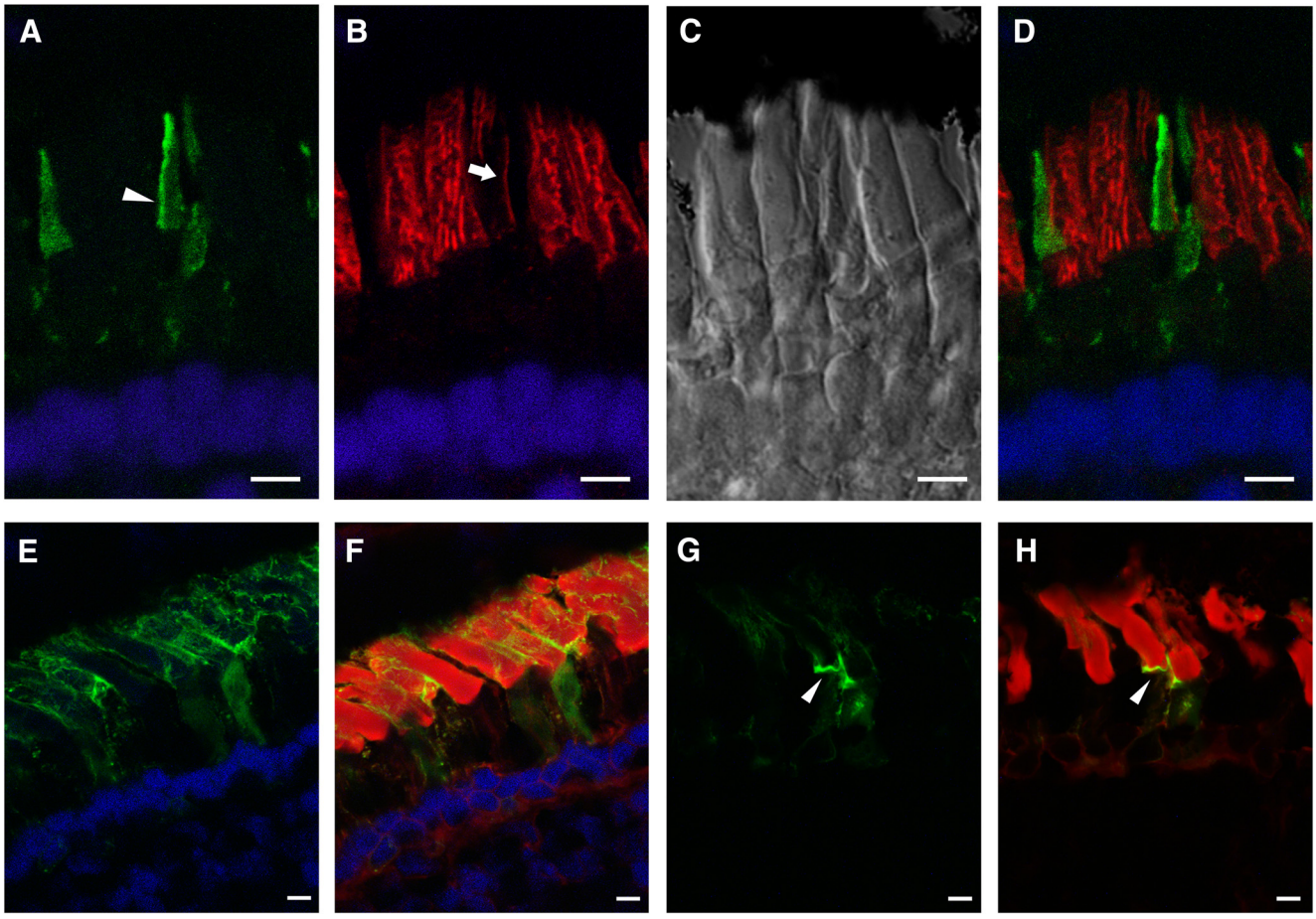

FIGURE 9. (**A–D**) xlProminin-1-hrGFP II expressed in transgenic *X. laevis* cones. Expression of the transgene is controlled by a newly isolated promoter XtCAP 1.9 for the *X. tropicalis* cone arrestin gene (see Supplementary Materials, http://www.iovs.org/lookup/suppl/doi:10.1167/iovs.11-8635/-/DCSupplemental). (**A**) The hrGFP II-tagged fusion protein localizes primarily to one side of COS (*arrowhead*). (**B**) The same section colabeled with anti–peripherin-2/rds antibody Xper5A11 (*red*). COS was labeled with the antibody and the labeling is confined to a thin area along one side of the COS (*arrow*). Longitudinal stripes in the adjacent rods result from the peripherin-2/rds localization along the aligned incisures of ROS disks. (**C**) Nomarski view of the same retina. (**D**) Superimposed image shows that xlProminin-1-hrGFP II resides on the side of the disk rims opposite peripherin-2/rds. Thus the transgenic hrGFP II-tagged protein expressed in cones distributes to the same sites as the endogenous protein we observed with anti–xlProminin-1 antibodies αPN and αPC. Nuclei are labeled with Hoechst 33342 dye (*blue*). (**E–H**) xlProminin-1-hrGFP II expressed in transgenic *X. laevis* rods. Expression of the transgene is controlled by a promoter XOP 1.3 for the *X. laevis* opsin gene. (**E**, **F**) The fusion protein is seen on the plasma membrane of both ROS and RIS (*green*) and occasionally is observed within the middle of the OS. Some fluorescence is seen within the RIS, presumably representing the trafficking of the newly synthesized protein. (**G**, **H**) The fusion protein is occasionally observed at the base of the ROS (*arrowhead*). Sections were counterstained with Texas Red-X conjugated wheat germ agglutinin (*red*) to visualize the ROS and post-Golgi membranes. Scale bars, 5 μm.

Our observation of the distinct labeling at the basal ROS by both anti–xlProminin-1 antibodies supports the model of disk morphogenesis in rods proposed by Steinberg et al., [9] in which the basal disks are open to the exterior environment and are structurally distinct from the closed distal disks in organization of their membrane proteins. This model was also supported by results of scanning electron microscopic observations and dye penetration into ROS basal disks.[55,56] However, the Steinberg et al.[9] model has recently been challenged by Chuang et al.,[57] who proposed an alternative mechanism of ROS disk morphogenesis by which no continuous lamellae exist in basal ROS disks.[57] They posited an exocytic model of disk morphogenesis with opsin-laden membranes budding from the apical plasma membrane of the RIS and fusing at the base of the ROS or passing through the cilium interior. However, opsin is barely detectable by electron microscope immunocytochemistry in the RIS plasma membrane adjacent to the basal ROS disks, whereas it is readily observed at high concentration in vesicles fusing at the base of the grooves of the periciliary ridge complex (PRC) and along the ciliary plasma membrane, and the same sites are labeled by incorporation of radioactive amino acids into opsin at an appropriate time point.[55,58] Moreover, opsin is detected along the ciliary plasma membrane but not in the interior of the connecting cilium.[55,58] In addition, rab8 localizes to the same site at the base of the grooves of the periciliary ridge complex,[59] and mutations of rab8 block fusion of the post-Golgi membranes transporting opsin to the grooves leading to pileup of rhodopsin transport carriers around the base of the PRC and to abnormal ROS formation.[60] A similar result is generated after the inhibition of phosphatidic acid hydrolase by propranolol, which also generated a redistribution of moesin and an accumulation of undocked post-Golgi rhodopsin transport carrier membranes near the base of the connecting cilium.[61] These results support the proposed role of the connecting cilium's plasmalemma as the sole means of transport of newly synthesized photopigment from the inner segment to the outer segment in rods.

We found proteolysis of xlProminin-1 in *X. laevis* tissues, a phenomenon that was not previously reported, and diurnal

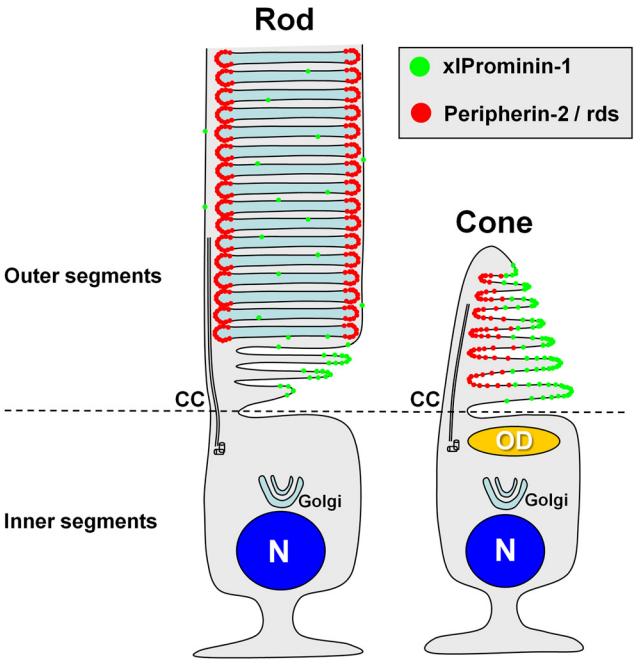

FIGURE 10. A model of differential distribution of xlProminin-1 and peripherin-2/rds in rod and cone photoreceptors. xlProminin-1 (*green*) distributes to the outer rims of open disk lamellae of COS and basal disks of ROS. Peripherin-2/rds, in contrast, distributes to the inner rim on the same side as the connecting cilium in COS and also to the entire rim of closed mature disks in ROS. Prominin-1 is also sparsely present throughout the entire disks of ROS. CC, connecting cilium; OD, oil droplet; N, nucleus.

variation of antibody labeling of xlProminin-1 at the basal ROS. Future directions may include studying the mechanism for xlProminin-1 localization in photoreceptors, measuring and comparing the turnover of xlProminin-1 in rods and cones, determining a circadian regulation of xlProminin-1 expression and localization in photoreceptors, positioning of the proteolysis site of xlProminin-1, and tracing the fate of its proteolytic products. Furthermore, the function of xlProminin-1 and the pathologic effects of prominin-1 mutations as identified in human patients could be investigated using the transgenic *X. laevis* approach and fluorescent protein tags, as was demonstrated in this study.

In summary, our finding of an asymmetrical and mutually exclusive distribution of xlProminin-1 and peripherin-2/rds provides insight into the origin of the structural differences between rods and cones, especially in lower vertebrates, and supports the Steinberg model of ROS disk morphogenesis.[9]

Acknowledgments

The authors thank Marc G. Pypaert (Yale University School of Medicine) and Arthur R. Hand and Maya Yankova (both at University of Connecticut Health Center) for help with the immunoelectron microscopy; Cheryl M. Craft (University of Southern California) for the anti–mouse blue (S) and green (M) cone opsin antibodies; and Orson L. Moritz (University of British Columbia) for helpful discussions on the manuscript.

References

1. Bowmaker JK. Visual pigments and colour vision in man and monkeys. *J R Soc Med.* 1981;74:348–356.
2. Young RW. Passage of newly formed protein through the connecting cilium of retina rods in the frog. *J Ultrastruct Res.* 1968;23:462–473.
3. Papermaster DS, Schneider BG, Besharse JC. Vesicular transport of newly synthesized opsin from the Golgi apparatus toward the rod outer segment: ultrastructural immunocytochemical and autoradiographic evidence in *Xenopus* retinas. *Invest Ophthalmol Vis Sci.* 1985;26:1386–1404.
4. Roepman R, Wolfrum U. Protein networks and complexes in photoreceptor cilia. *Subcell Biochem.* 2007;43:209–235.
5. Yau KW. Phototransduction mechanism in retinal rods and cones: the Friedenwald Lecture. *Invest Ophthalmol Vis Sci.* 1994;35:9–32.
6. Wald G. The molecular basis of visual excitation. *Nature.* 1968;219:800–807.
7. Lamb TD, Collin SP, Pugh EN Jr. Evolution of the vertebrate eye: opsins, photoreceptors, retina and eye cup. *Nat Rev.* 2007;8:960–976.
8. Nathans J, Thomas D, Hogness DS. Molecular genetics of human color vision: the genes encoding blue, green, and red pigments. *Science.* 1986;232:193–202.
9. Steinberg RH, Fisher SK, Anderson DH. disk morphogenesis in vertebrate photoreceptors. *J Comp Neurol.* 1980;190:501–508.
10. Eckmiller MS. Cone outer segment morphogenesis: taper change and distal invaginations. *J Cell Biol.* 1987;105:2267–2277.
11. Cohen AI. New details of the ultrastructure of the outer segments and ciliary connectives of the rods of human and macaque retinas. *Anat Rec.* 1965;152:63–79.
12. Cohen AI. New evidence supporting the linkage to extracellular space of outer segment saccules of frog cones but not rods. *J Cell Biol.* 1968;37:424–444.
13. Laties AM, Liebman PA. Cones of living amphibian eye: selective staining. *Science.* 1970;168:1475–1477.
14. Anderson DH, Fisher SK, Steinberg RH. Mammalian cones: disk shedding, phagocytosis, and renewal. *Invest Ophthalmol Vis Sci.* 1978;17:117–133.
15. Besharse JC, Hollyfield JG, Rayborn ME. Turnover of rod photoreceptor outer segments, II: membrane addition and loss in relationship to light. *J Cell Biol.* 1977;75:507–527.
16. Young RW, Droz B. The renewal of protein in retinal rods and cones. *J Cell Biol.* 1968;39:169–184.
17. Young RW. Visual cells and the concept of renewal. *Invest Ophthalmol Vis Sci.* 1976;15:700–725.
18. Young RW. The renewal of photoreceptor cell outer segments. *J Cell Biol.* 1967;33:61–72.
19. Young RW, Bok D. Participation of the retinal pigment epithelium in the rod outer segment renewal process. *J Cell Biol.* 1969;42:392–403.
20. Young RW, Bok D. Autoradiographic studies on the metabolism of the retinal pigment epithelium. *Invest Ophthalmol.* 1970;9:524–536.
21. Weigmann A, Corbeil D, Hellwig A, Huttner WB. Prominin, a novel microvilli-specific polytopic membrane protein of the apical surface of epithelial cells, is targeted to plasmalemmal protrusions of non-epithelial cells. *Proc Natl Acad Sci U S A.* 1997;94:12425–12430.
22. Miraglia S, Godfrey W, Yin AH, et al. A novel five-transmembrane hematopoietic stem cell antigen: isolation, characterization, and molecular cloning. *Blood.* 1997;90:5013–5021.
23. Yin AH, Miraglia S, Zanjani ED, et al. AC133, a novel marker for human hematopoietic stem and progenitor cells. *Blood.* 1997;90:5002–5012.
24. Maw MA, Corbeil D, Koch J, et al. A frameshift mutation in prominin (mouse)-like 1 causes human retinal degeneration. *Hum Mol Genet.* 2000;9:27–34.
25. Zacchigna S, Oh H, Wilsch-Brauninger M, et al. Loss of the cholesterol-binding protein prominin-1/CD133 causes disk dysmorphogenesis and photoreceptor degeneration. *J Neurosci.* 2009;29:2297–2308.
26. Yang Z, Chen Y, Lillo C, et al. Mutant prominin 1 found in patients with macular degeneration disrupts photoreceptor disk morphogenesis in mice. *J Clin Invest.* 2008;118:2908–2916.
27. Permanyer J, Navarro R, Friedman J, et al. Autosomal recessive retinitis pigmentosa with early macular affectation caused by premature truncation in PROM1. *Invest Ophthalmol Vis Sci.* 2010;51:2656–2663.

28. Zelhof AC, Hardy RW, Becker A, Zuker CS. Transforming the architecture of compound eyes. *Nature.* 2006;443:696–699.
29. Han Z, Papermaster DS. Identification of three prominin homologs and characterization of their messenger RNA expression in *Xenopus laevis* tissues. *Mol Vis.* 2011;17:1381–1396.
30. Fiedler M, Horn C, Bandtlow C, Schwab ME, Skerra A. An engineered IN-1 F(ab) fragment with improved affinity for the Nogo-A axonal growth inhibitor permits immunochemical detection and shows enhanced neutralizing activity. *Protein Eng.* 2002;15:931–941.
31. Poirier F, Lawrence D, Vigier P, Jullien P. A ts T mutant of Schmidt Ruppin strain of Rous sarcoma virus restricted at 39.5 degrees C for the morphological transformation and the tumorigenicity of chicken embryo fibroblasts. *Int J Cancer.* 1982;29:69–76.
32. Papermaster DS, Converse CA, Siuss J. Membrane biosynthesis in the frog retina: opsin transport in the photoreceptor cell. *Biochemistry.* 1975;14:1343–1352.
33. Corbeil D, Fargeas CA, Huttner WB. Rat prominin, like its mouse and human orthologues, is a pentaspan membrane glycoprotein. *Biochem Biophys Res Commun.* 2001;285:939–944.
34. Laemmli UK. Cleavage of structural proteins during the assembly of the head of bacteriophage T4. *Nature.* 1970;227:680–685.
35. Peterson JJ, Tam BM, Moritz OL, et al. Arrestin migrates in photoreceptors in response to light: a study of arrestin localization using an arrestin-GFP fusion protein in transgenic frogs. *Exp Eye Res.* 2003;76:553–563.
36. Moritz OL, Tam BM, Knox BE, Papermaster DS. Fluorescent photoreceptors of transgenic *Xenopus laevis* imaged in vivo by two microscopy techniques. *Invest Ophthalmol Vis Sci.* 1999;40:3276–3280.
37. Kozak M. An analysis of vertebrate mRNA sequences: intimations of translational control. *J Cell Biol.* 1991;115:887–903.
38. Kroll KL, Amaya E. Transgenic *Xenopus* embryos from sperm nuclear transplantations reveal FGF signaling requirements during gastrulation. *Development.* 1996;122:3173–3183.
39. Papermaster DS. Preparation of retinal rod outer segments. *Methods Enzymol.* 1982;81:48–52.
40. Kedzierski W, Moghrabi WN, Allen AC, et al. Three homologs of rds/peripherin in *Xenopus laevis* photoreceptors that exhibit covalent and non-covalent interactions. *J Cell Sci.* 1996;109(pt 10):2551–2560.
41. Loewen CJ, Moritz OL, Tam BM, Papermaster DS, Molday RS. The role of subunit assembly in peripherin-2 targeting to rod photoreceptor disk membranes and retinitis pigmentosa. *Mol Biol Cell.* 2003;14:3400–3413.
42. Papermaster DS, Schneider BG, Zorn MA, Kraehenbuhl JP. Immunocytochemical localization of opsin in outer segments and Golgi zones of frog photoreceptor cells: an electron microscope analysis of cross-linked albumin-embedded retinas. *J Cell Biol.* 1978;77:196–210.
43. Moritz OL, Tam BM, Papermaster DS, Nakayama T. A functional rhodopsin-green fluorescent protein fusion protein localizes correctly in transgenic *Xenopus laevis* retinal rods and is expressed in a time-dependent pattern. *J Biol Chem.* 2001;276:28242–28251.
44. Arikawa K, Molday LL, Molday RS, Williams DS. Localization of peripherin/rds in the disk membranes of cone and rod photoreceptors: relationship to disk membrane morphogenesis and retinal degeneration. *J Cell Biol.* 1992;116:659–667.
45. Goldberg AF, Loewen CJ, Molday RS. Cysteine residues of photoreceptor peripherin/rds: role in subunit assembly and autosomal dominant retinitis pigmentosa. *Biochemistry.* 1998;37:680–685.
46. Braekevelt CR, Smith SA, Smith BJ. Photoreceptor fine structure in *Oreochromis niloticus L.* (*Cichlidae*; *Teleostei*) in light- and dark-adaptation. *Anat Rec.* 1998;252:453–461.
47. Edrington TCT, Lapointe R, Yeagle PL, Gretzula CL, Boesze-Battaglia K. Peripherin-2: an intracellular analogy to viral fusion proteins. *Biochemistry.* 2007;46:3605–3613.
48. Boesze-Battaglia K, Stefano FP, Fitzgerald C, Muller-Weeks S. ROM-1 potentiates photoreceptor specific membrane fusion processes. *Exp Eye Res.* 2007;84:22–31.
49. Damek-Poprawa M, Krouse J, Gretzula C, Boesze-Battaglia K. A novel tetraspanin fusion protein, peripherin-2, requires a region upstream of the fusion domain for activity. *J Biol Chem.* 2005;280:9217–9224.
50. Boesze-Battaglia K, Goldberg AF, Dispoto J, Katragadda M, Cesarone G, Albert AD. A soluble peripherin/Rds C-terminal polypeptide promotes membrane fusion and changes conformation upon membrane association. *Exp Eye Res.* 2003;77:505–514.
51. Boesze-Battaglia K. Fusion between retinal rod outer segment membranes and model membranes: functional assays and role for peripherin/rds. *Methods Enzymol.* 2000;316:65–86.
52. Boesze-Battaglia K, Lamba OP, Napoli AA, Jr., Sinha S, Guo Y. Fusion between retinal rod outer segment membranes and model membranes: a role for photoreceptor peripherin/rds. *Biochemistry.* 1998;37:9477–9487.
53. Kedzierski W, Weng J, Travis GH. Analysis of the rds/peripherin-.rom1 complex in transgenic photoreceptors that express a chimeric protein. *J Biol Chem.* 1999;274:29181–29187.
54. Matsumoto B, Besharse JC. Light and temperature modulated staining of the rod outer segment distal tips with Lucifer yellow. *Invest Ophthalmol Vis Sci.* 1985;26:628–635.
55. Peters KR, Palade GE, Schneider BG, Papermaster DS. Fine structure of a periciliary ridge complex of frog retinal rod cells revealed by ultrahigh resolution scanning electron microscopy. *J Cell Biol.* 1983;96:265–276.
56. Laties AM, Bok D, Liebman P. Procion yellow: a marker dye for outer segment disk patency and for rod renewal. *Exp Eye Res.* 1976;23:139–148.
57. Chuang JZ, Zhao Y, Sung CH. SARA-regulated vesicular targeting underlies formation of the light-sensing organelle in mammalian rods. *Cell.* 2007;130:535–547.
58. Papermaster DS, Schneider BG, DeFoe D, Besharse JC. Biosynthesis and vectorial transport of opsin on vesicles in retinal rod photoreceptors. *J Histochem Cytochem.* 1986;34:5–16.
59. Deretic D, Huber LA, Ransom N, Mancini M, Simons K, Papermaster DS. rab8 in retinal photoreceptors may participate in rhodopsin transport and in rod outer segment disk morphogenesis. *J Cell Sci.* 1995;108(pt 1):215–224.
60. Moritz OL, Tam BM, Hurd LL, Peranen J, Deretic D, Papermaster DS. Mutant rab8 Impairs docking and fusion of rhodopsin-bearing post-Golgi membranes and causes cell death of transgenic *Xenopus* rods. *Mol Biol Cell.* 2001;12:2341–2351.
61. Deretic D, Traverso V, Parkins N, Jackson F, Rodriguez de Turco EB, Ransom N. Phosphoinositides, ezrin/moesin, and rac1 regulate fusion of rhodopsin transport carriers in retinal photoreceptors. *Mol Biol Cell.* 2004;15:359–370.